Crystal Structure of Cardiotoxin V from Taiwan Cobra Venom: pH-Dependent Conformational Change and a Novel Membrane-Binding Motif Identified in the Three-Finger Loops of P-Type Cardiotoxin[†,‡]

Yuh-Ju Sun,[§] Wen-guey Wu,[||] Chien-Min Chiang,[||] A-Yen Hsin,[§] and Chwan-Deng Hsiao*[,§]

Crystallography Laboratory, Institute of Molecular Biology, Academia Sinica, Taipei, Taiwan 11529, and Structural Biology Group, Department of Life Sciences, National Tsing Hua University, Hsinchu, Taiwan 30043

Received October 16, 1996; Revised Manuscript Received December 23, 1996[⊗]

ABSTRACT: The crystal structure of cardiotoxin V from Taiwan cobra venom (CTX A5) has been solved at pH 8.5 and refined to an *R*-factor of 20.7% for 7013 reflections [$>2\sigma(F)$] between 8- and 2.19-Å resolution. The refined model shows that CTX A5 exists as a dimer. The assembly consists of 974 non-hydrogen atoms from 124 residues and 73 water molecules. The global monomeric structure is similar to that determined by NMR at pH 3.7, characterized by a core formed by two β-sheets connected with three-finger loops. However, local conformational differences are detected in two functionally important regions, loops I and II. A disparity between the NMR and X-ray structure of CTX A5 is detected near the tip of loop I and can be attributed to the difference in the protonation state of His4 at different pH, resulting in a reorientation of the His4 imidazole ring. A concerted motion of amino acid side chains located near His4 is detected and possibly contributes to the pH-dependent binding ability of CTX A5 to phospholipid model membranes. The second difference, detected at the tip of loop II, is due to the hydrophobic contact between CTX dimers in the crystal packing and the interaction of water molecules with amino acid residues in the loop II region of the CTX containing Pro31 (P-type CTX). This interaction forces loop II into a more rigid Ω shape bridging the main chain at positions 27 and 34, contradictory to the flexible, tapering shape detected by NMR. Thus, a novel continuous hydrophobic column capable of binding to and possibly penetrating the membrane lipid bilayer is formed by the tips of the three-finger loops. In this respect, the X-ray crystal structure of CTX A5 may represent the CTX structure in the membrane-binding mode.

The three-dimensional structures of snake cardiotoxins (CTXs) have been extensively studied. Rees and co-workers have elucidated two crystal structures (Rees et al., 1990; Bilwes et al., 1994). In addition, four solution structures for various CTXs have been determined by NMR (Table 1). The reported structures of CTX monomers are similar. They consist of a large triple-stranded, antiparallel β-sheet connected by loops II and III and a short double-stranded β-sheet connected by loop I. A core is formed by four disulfide bonds in the bottom region of the CTX molecules with the three loops protruding in the opposite direction.

The most significant conformational differences detected among these structures are located at the tips of loops I and II, probably due to the flexibility at these regions. However, whether the observed conformational differences have any relevance on the functional roles of various CTX homologues has not been addressed. More interestingly, two distinct types of CTXs, i.e., P- and S-type, can be distinguished by the presence of Pro31 and Ser29, respectively, near the tip of loop II (Chien et al., 1994). P-type CTXs interact more strongly with membrane than S-type CTXs, but the structural and functional roles of these two residues remain to be determined.

Fluorescence and NMR studies indicate that loops I, II, and III are perturbed upon micelle association (Chien et al., 1994; Dauplais et al., 1995). Results from infrared, circular dichroism, and NMR spectroscopic studies have suggested that lipid association can induce an increase in the β-sheet content of CTXs at the expense of the random-coil conformation (Surewicz et al., 1988; Chien et al., 1994; Dauplais et al., 1995; Chiang et al., 1996a). This raises an interesting question of whether the conformation of CTX in solution or in the crystal is comparable to that of CTX in the cell membranes.

Cardiotoxin V from Taiwan cobra (CTX A5)[1] is a P-type CTX. It can cause vesicle aggregation/fusion around the phospholipid transition temperatures (Chien et al., 1991). The NMR solution structure of this toxin at pH 3.7 has been reported (Singhal et al., 1993). CTX A5 binds to phospholipid in a pH-dependent manner and an apparent pK_a of 6.0 has been assigned (Chiang et al., 1996a). Recently, Chiang et al. (1996a,b) suggested that His4 on CTX A5 is protonated, resulting in a local conformational change. In addition, there is a differential in surface charge distribution on CTX A5.

[†] This research was supported by Academia Sinica and in part by Grants NSC 85-2311-B001-096 (to C.-D.H.) and NSC 85-2113-M007-035Y (to W.-g.W.) from National Science Council, Taiwan.

[‡] The coordinates have been deposited in the Brookhaven Protein Data Bank (reference number 1KXI).

* Author to whom correspondence should be addressed. Tel: 886-02-788-2743. Fax: 886-02-782-6085. Email: MBHSIAO@CCVAX.SINICA.EDU.TW.

[§] Academia Sinica.

[||] National Tsing Hua University.

[⊗] Abstract published in *Advance ACS Abstracts,* February 15, 1997.

[1] Abbreviations: CTX A5, cardiotoxin V from *Naja naja atra*; NMR, nuclear magnetic resonance; PC, phosphatidylcholine.

S0006-2960(96)02594-9 CCC: $14.00

Table 1: Amino Acid Sequences and Three-Dimensional Structures of Snake Cardiotoxins[a]

CTX	Amino acid sequences	Method	pH	Reference	Code
M3	LKC-NKLIPI AYKTCP**E**GKN LCYKMMLASK -KMVPVKRGC INVCPKNSAL VKYVCCSTDR CN	X-ray	7.2	Rees et al.,1990; 1987	1CDT
M1	LKC-NQLIPP FWKTCP**K**GKN LCYKMTMRAA P-MVPVKRGC IDVCPKSSLL IKYMCCNTNK CN	NMR	6.0	O'Connel et al.,1993	1CCX
Tg	LKC-NQLIPP FWKTCP**K**GKN LCYKMTMRAA P-MVPVKRGC IDVCPKSSLL IKYMCCNTDK CN	NMR	3.5	Gilquin et al., 1993	1CXN
Tg	LKC-NQLIPP FWKTCP**K**GKN LCYKMTMRAA P-MVPVKRGC IDVCPKSSLL IKYMCCNTDK CN	X-ray	4.5	Bilwes et al., 1994	1TGX
A5	LKCHNTQLPF IYKTCP**E**GKN LCFKATLKKF PLKFPVKRGC ADNCPKNSAL LKYVCCSTDK CN	NMR	3.7	Singhal et al., 1993	1CVO
A5	LKCHNTQLPF IYKTCP**E**GKN LCFKATLKKF PLKFPVKRGC ADNCPKNSAL LKYVCCSTDK CN	X-ray	8.5	Sun et al., This work	1KXI
A3	LKC-NKLVPL FYKTCP**A**GKN LCYKMFMVAT P-KVPVKRGC IDVCPKSSLL VKYVCCNTDR CN	NMR	3.0	Bhaskaran et al., 1994	2CRT
A1	LKC-NKLIPI ASKTCP**A**GKN LCYKMFMMSD -LTIPVKRGC IDVCPKNSLL VKYVCCNTDR CN	NMR	5.6	Jahnke et al., 1994	2CDX
A2	LKC-NKLVPL FYKTCP**A**GKN LCYKMFMVSN -LTVPVKRGC IDVCPKNSAL VKYVCCNTDR CN	NMR	3.0	Bhaskaran et al., 1994	1CAR

[a] CTX Tg represents toxin γ from *Naja nigricollis* venom. CTX A and CTX M represent cardiotoxins from *Naja naja atra* and *Naja mossambica mossambica* venom, respectively. Tg differs from M1 by only one amino acid residue, at position 49. A5 consists of titratable His-4 with pK_a* near 5.6. In general, P-type CTXs (CTXs with Pro31) exhibit greater phospholipid binding activity than S-type CTXs (CTXs with Ser29). The sequence listed for CTX A1 is that used for NMR determination but differs from the sequence originally determined. There is an amino acid inversion between Asn47 and Ser48.

Together, these two factors ensure the localization of the protonated His4 at the membrane−water interface, with the implication that this residue plays a role in the binding of CTX A5 to the phosphatidylcholine (PC) monolayers. The molecular details of this conformational change, however, are unknown. Out of 46 CTXs with known sequences, approximately 19 of them have a histidine at position 4 (Dufton & Hider, 1991; Chien et al., 1994). Determination of the X-ray crystal structure of CTX A5 near physiological pH should provide additional structural information on this class of CTX molecules.

We report here the X-ray crystal structure of CTX A5 at 2.19-Å resolution. The structure shows dimeric assembly at pH 8.5. Conformational differences between the structure determined by NMR at pH 3.7 and by crystallography at pH 8.5 are localized at two functionally important regions in loops I and II. Due to the crystal packing and physiological pH condition, the X-ray structure represents a good model for the membrane-binding state of the P-type CTXs. The results also provide a structural explanation for the pH-dependent binding of CTX A5 to membrane phospholipids and suggest a novel membrane-spanning motif formed by the three-finger loops.

MATERIALS AND METHODS

Isolation and Crystallization. CTX A5 was purified as previously reported (Chien et al., 1991, 1994). Briefly, CTX A5 was isolated from the venom of *Naja naja atra* on a SP-Sephadex C-25 (Sigma) ion-exchange column and further on an Ultrapore reverse-phase C-8 (5-mm) column using a phosphate buffer system (10 mM NaH_2PO_4 and 10 mM Na_2SO_4, pH 4) and eluted with an acetonitrile gradient.

The crystals of CTX A5 were grown by the hanging drop vapor diffusion method at 18 °C from 3-μL droplets of protein solution (10 mg/mL) containing 10% PEG 4000, 0.15 M Li_2SO_4, and 0.1 M Tris-HCl (pH 8.5). The protein solution was placed on the wall of a siliconized cover slide against a reservoir of the above buffer containing 20% PEG 4000. Small plate-shape crystals appeared in a day and grew to a size of 0.4 mm × 0.3 mm × 0.1 mm within 3 weeks. The crystals were found to have unit cell dimensions $a = b = 43.3$ Å, $c = 147.8$ Å with $\alpha = \beta = \gamma = 90.0°$. The systematic absences (00l except for $l = 4n$ and h00 except for $h = 2n$) and Laue symmetry of the diffraction pattern (4/*mmm*) indicate that the space group is $P4_12_12$ or $P4_32_12$.

The crystals diffract to a 2.19-Å resolution and contain 2 molecules (one dimer) per asymmetric unit. The value of V_m (Matthews, 1968) is calculated to be 2.47 Å^3/Da and the solvent content is estimated to be 50%. The self-rotation search (Fitzgerald, 1988) (10−4 Å, Patterson cutoff of 23.5 Å) showed only peaks corresponding to the directions of crystallographic axes. However, a large peak (weighing about 50% of the origin peak) appeared in one of the Harker sections at $U = 0.0$, $V = 0.0$, and $W = 0.5$ in the native Patterson map. This peak suggests the possibility that molecules related by a translation of half a unit cell along the *z* axis with a corresponding unit cell dimension half of the reported value of 147.8 Å may be present. We therefore analyzed carefully the entire data set and found that most of the $l = 2n + 1$ reflections are still present with intensities occasionally even stronger than those of the $l = 2n$ reflections. In addition, the reduction of the z axis from 147.8 to 73.9 Å makes it difficult to index many reflections. We conclude that the unit cell dimensions of $a = b = 43.3$ Å, $c = 147.8$ Å are indeed correct. This result also indicates that the dimeric local 2-fold axis is parallel to the 4-fold crystallographic axis.

Data Collection and Processing. X-ray intensity data were collected from a single crystal using CuK_α radiation on a Rigaku R-AXIS II imaging plate system operated at 50 kV and 80 mA. The program DENZO (Otwinowski, 1993) was used to index images, integrate intensities, and scale data. A total of 38 418 observations were recorded and reduced to 7280 unique reflections with an R_{merge} of 8% based on intensity between symmetry-related reflections. The final data set used for the refinement is summarized in Table 2. The merged data set corresponds to 91.7% of the complete possible data up to 2.19-Å resolution. The outermost shell of resolution is 82.2% complete.

Structure Determination and Refinement. The 3D structure of CTX A5 was determined by the molecular replace-

Table 2: Summary of Diffraction Data and Refinement

resolution of data	2.19 Å
number of data collected	38 418
number of unique data	7280
completeness (up to 2.19 Å)	91.7%
completeness of the outermost shell	82.2%
$R_{sym}(I)^a$	8.0%
total number of atoms	974
number of solvent molecules	73
rms deviations from ideal geometry	
bond lengths	0.01 Å
bond angles	1.6°
R-factor for 7013 reflections (8.0∼2.19 Å, 2σ)	0.207

[a] $R_{sym}(I) = \Sigma_h\Sigma_i|I_i - I|/\Sigma_h\Sigma_i I$, where I is the mean intensity of the i observations of reflection h.

ment method. In initial studies, the NMR solution structure of CTX A5 determined at pH 3.7 (Singhal et al., 1993) was used as a search model with several molecular replacement software packages without success. Therefore, a homologous protein, CTX M3, whose structure has been resolved at 2.5 Å (Rees et al., 1990) was used as template. The probe model was constructed by substituting the side chains of CTX M3 with those from the CTX A5 sequence, and the flexible loops I and II (residues 6−12 and 28−34) were excluded from the molecular replacement calculation. Molecular replacement was carried out using the AMoRe package (Navaza, 1994). The search model was placed in a *P*1 cell with $a = b = c = 60$ Å and $\alpha = \beta = \gamma = 90°$. The shell of data between 8.0 and 4.0 Å and a 17-Å radius sphere were used for all the rotation and translation function calculations. To determine the correct enantiomorph, both $P4_12_12$ and $P4_32_12$ space groups were used for molecular replacement calculations. However, only the $P4_12_12$ space group showed a significant translation solution.

Structure refinement was carried out using the X-PLOR program package (Brunger, 1990). The first step was a rigid-body refinement. The probe model was used as a group to optimize the orientational and translational parameters. The *R*-factor after rigid-body refinement was 42%. The second step was an atomic position refinement by conjugate gradient minimization. The two molecules of the asymmetric unit were treated by noncrystallographic symmetry restraints. The *R*-factor was reduced to 34% in the 8−2.7-Å resolution range after these two steps.

A $2|F_o| - |F_c|$ electron density map was then calculated to include the contribution of residues omitted from loops I and II. After these loops were rebuilt, the simulated annealing (SA) protocol was used with initial temperature of 3000 K. The final temperature of 300 K was reached by gradually lowering the temperature by 25 K/50 dynamics steps. The two molecules of the asymmetric unit were then refined independently. Only half of the relative weight (W_A) was used to reduce the possibility of overfitting the model during the SA refinement. The *R*-factor was dropped to 23.3% after SA refinement.

The entire molecule was rebuilt by examining the "omit" difference Fourier maps. The annealed omit map protocol was used initially to generate the omit maps. Approximately 5% of the molecules (equivalent to three successive residues from both monomers) were deleted in generating the annealed omit maps. The remaining atoms were used to calculate the structure factors (F_c) and phases (α_c). Difference

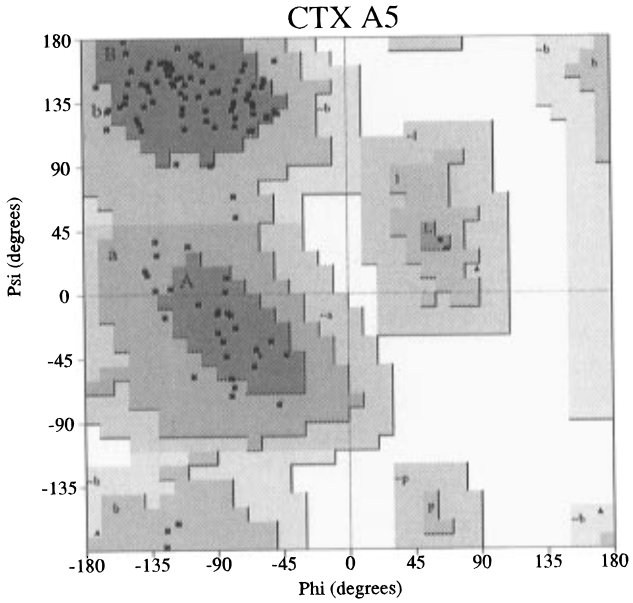

FIGURE 1: Ramachandan plot of the refined 2.19-Å CTX A5 structure. Glycine residues are indicated by triangles and all other residues by squares (program PROCHECK; Laskowski et al., 1993).

Fourier maps were then computed using ($2|F_o| - |F_c|$, α_c) and ($|F_o| - |F_c|$, α_c) as coefficients. The process was systematically continued until sufficient omit maps were generated to account for the entire molecule. Refinement was continued by gradually increasing the resolution of the data from 2.7 to 2.19 Å, and the *R*-factor remained at 24%.

The water molecules were located by searching the $|F_o| - |F_c|$ difference Fourier map for positive density with peak height above 2.5σ and within H-bonding distance (2.5−3.5 Å) of potential donor or acceptor atoms (O and N atoms) of the protein. During the refinement, the occupancies of these water molecules (oxygen atoms) were fixed at 1.0 while the locations and the temperature factors were refined. Solvent molecules exhibiting temperature factors above 50 Å^2 after several cycles of refinement were excluded from the model.

After this calculation, the ϕ, ψ angles of the polypeptidic chain of both monomers fall in reasonable regions in a Ramachandran plot; therefore, the full relative weight (W_A) was used in the final refinement. After the final refinement process, the *R*-factor is 20.7% for the 7013 reflections [$>2\sigma(F)$] from 8.0 to 2.19 Å. The R_{free} value (Brunger, 1992) for the 765 randomly selected reflections [$2\sigma(F)$] that were excluded from the refinement process is 30.5%. The ideal bond distances and the bond angles have rms deviations of 0.010 Å and 1.6°, respectively. The final model of CTX A5 contains 974 non-hydrogen atoms, including 73 oxygen atoms from water molecules. The ϕ, ψ angles of the polypeptide chain are shown on the Ramachandran plot as depicted in Figure 1. The $2|F_o| - |F_c|$ omitted density maps of loop II from both monomers superimposed with the final refined model are shown in Figure 2.

NMR Chemical Shift Analysis. The electrostatic (δ_{elec}) and ring-current shift (δ_{rc}) effects of the protonated/unprotonated imidazole on the chemical shifts of the CTX A5 amide protons were calculated according to Williamson and Asakura (1993) and Asakura et al. (1995). The ^{1}H NMR chemical shift differences data between pH 7.0 and 5.1 were obtained from Chiang et al. (1996a). Comparison between the experimental and theoretical data was performed by assuming

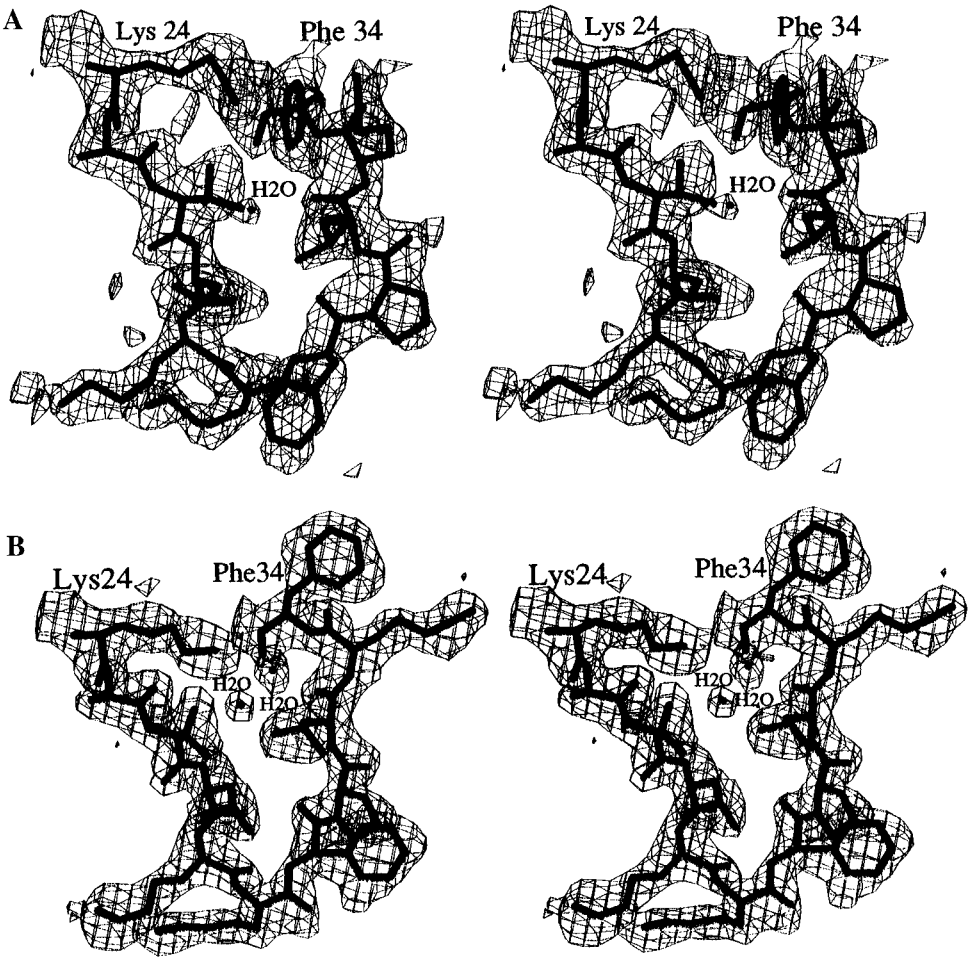

FIGURE 2: Stereo views of the residue-deleted (residues 30−34) $2|F_o| - |F_c|$ map with the final refined model superimposed. The maps are contoured at 1σ. Panels A and B correspond to monomers A and B, respectively.

that the imidazole ring may rotate by 90° during the protonation/unprotonation process. Briefly, the electrostatic contribution to the chemical shift differences of the studied NH protons was calculated using the equation $\delta_{elec} = \epsilon_1 E_z + \epsilon_2 E^2$. The values of ϵ_1 and ϵ_2 were estimated to be about 3.3 and 0 on the basis of the chemical shift difference detected upon protonation/deprotonation of Glu17 and Asp42. The electric charge of the imidazole ring was assumed to distribute equally at the N(ϵ^2) and H(ϵ^2) atomic positions [see Creighton (1993) for notation of atomic positions]. The ring-current effect of the imidazole ring on the chemical shift of NH protons was estimated from the equation $\delta_{rc} = iBG(r)$, where $G(r)$ was calculated according to the Haigh−Mallion model. The coefficient of B was fixed at 0.88, conforming with Osapay and Case (1991). The distances between the imidazole ring and the studied amide protons were obtained from the present study. Only the rotation of the χ_2 angle (-C_β-Cγ-) was considered in estimating the reorientational effect of the imidazole ring on the chemical shift of the NH protons.

RESULTS

CTX A5 Has a Three-Finger Motif with a Water Binding Central Loop. CTX A5 shares the common three-finger motif and molecular shape with other snake toxins such as neurotoxins or CTXs (Figure 3). CTX A5 assumes a flat shape with dimensions of approximately 34 Å × 24 Å × 15 Å. The secondary structure is exclusively of β-sheet type. It consists of three loops termed loops I (residues 5−13), II (residues 27−36), and III (residues 48−52) that protrude from a central core, tightened by four disulfide linkages (Cys3−Cys22, Cys15−Cys40, Cys44−Cys55, and Cys56−Cys61).

CTX A5 forms dimers in the X-ray crystal structure with an important solvent site near the tip of loop II. Solvation stretches this loop into an Ω shape that can be observed in both monomers. Monomer A has a single water molecule that forms three H-bonds with Leu27, Leu32, and Phe34 in this loop (Figure 4A). Two water molecules were detected in this region for monomer B to form three H-bonds with three residues as in monomer A (Figure 4B). Consequently, the water molecules stretch the loop II of monomer B to a farther extent than monomer A.

NMR studies have not detected the existence of water molecules within loop II. However, a similar water binding site has been observed in the crystal structure of the toxin γ central loop, a P-type CTX (Bilwes et al., 1994; Table 3). There are three structural features regarding the water binding site of CTX molecule that warrant further attention. First, most of the amino acid residues wrapping around the water molecule are hydrophobic. The formation of an extended hydrophobic loop is more pronounced in CTX A5 than in toxin γ due to the insertion of a hydrophobic leucine at position 32. Second, the rigid ring structure of Pro31 apparently has significant effects on the polypeptide backbone conformation that allow the interaction of water with

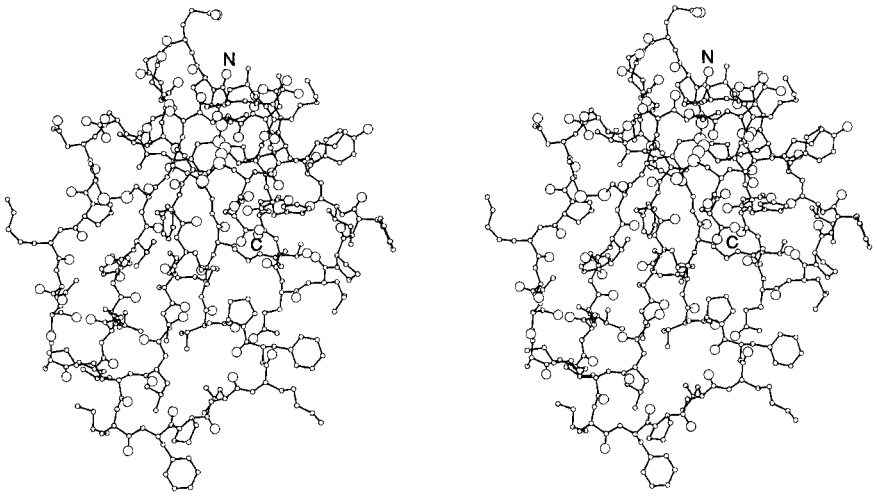

FIGURE 3: Stereoscopic view of the overall structure of CTX A5 monomer A with side chains.

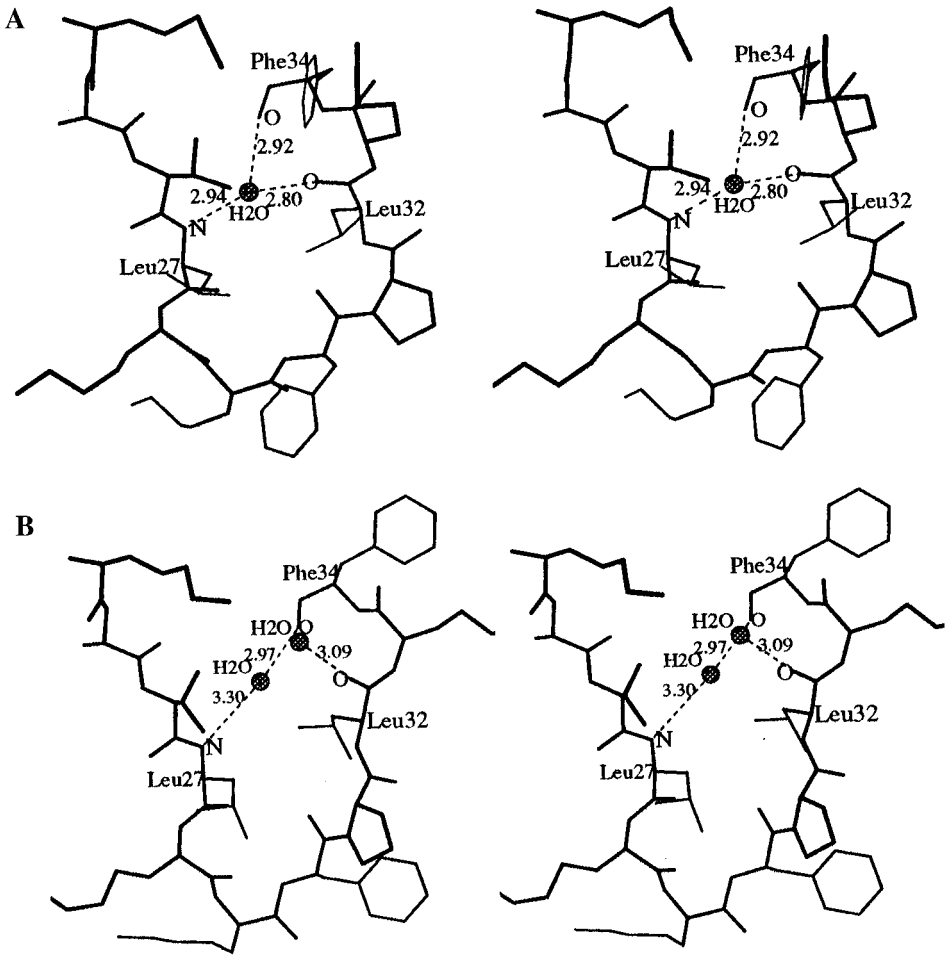

FIGURE 4: Stereo views of water molecules in loop II: (A) monomer A with three H-bonds involving one water molecule and (B) monomer B with three H-bonds involving two water molecules.

the carbonyl group of the main chain. Third, examination of the crystal packing suggests that the CTX dimers also contact each other via hydrophobic regions in loop II. Apparently, maximization of the hydrophobic contact plays a role in the formation of the Ω loop structure. Details of the crystal packing and the dimeric structure are presented in the next section.

The Dimer. The CTX A5 dimer is composed of two crystallographically independent molecules with essentially identical folding, but the polypeptide chain configuration differs significantly in the external loops. The superimposed C_α positions of the two CTX monomers show an rms difference of 0.54 Å. The greatest conformational differences between these two molecules occur at residues 28−36 (Figure 5A), which are located at the tip of loop II. Interestingly, the most significant structural difference is detected at Lys33, which is located in the water binding loop (Figure 4). Smaller differences are observed around residues 7−10 of loop I, residues 47−49 of loop III, and residues 17−19. These differences arise partially from chain flexibility and the crystal packing environment, as indicated by the higher thermal parameters for these residues (Figure 5B)

Table 3: Comparison of Hydrogen Bonds within the Water-Binding Loop[a]

CTX A5				toxin γ		
	monomer A[b]	monomer B		monomer 1	monomer 2	monomer 3
Leu27 N	2.94	3.30	Met26 N[c]	2.84	3.04	2.90
			Ala29 O[c]	2.89	3.01	2.84
Leu32 O	2.80	(3.09)[d]				
Phe34 O	2.92	2.97	Val32 O[c]	2.67	2.70	2.77

[a] Leu27 in CTX A5 can be considered to correspond to Met26 in toxin γ due to insertion of histidine at position 4. Similarly, Phe34 in CTX A5 corresponds to Val32 in toxin γ due to additional amino acid Leu32. [b] The solvent molecule involved in H-bond formation is similar to that in toxin γ. [c] Only one solvent molecule is observed to form H-bonds involving the indicated three positions. A similar solvent molecule is observed in all three monomers. [d] Two solvent molecules are involved in H-bond formation in monomer B and the solvent molecule involved in this H-bond is different from that in monomer A.

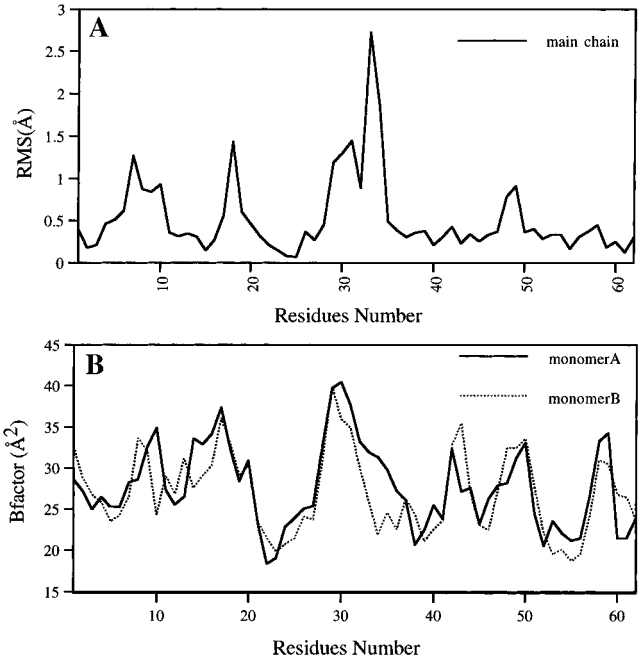

FIGURE 5: (A) Rms difference of the main-chain backbone between the two monomeric structures in the CTX A5 dimer. (B) Average temparature factor of main-chain atoms for each residue.

and the number of molecular contacts. For instance, there are 64 and 20 individual interactions ranging from 2.3 to 4.1 Å for residues 28−36 (loop II) of monomers B and A, respectively.

The dimeric interactions of CTX A5 are fairly strong. Nine H-bonds hold the two molecules together (Table 4) with a pseudo-2-fold symmetry. These H-bonds are formed between residues (Cys44, Pro45, Lys46, Asn47, Cys55, Ser57, and Thr58) located at the outer strand of loop III (Figure 6A,C). The intermolecular contacts involve side chains and two short CO···NH main-chain H-bonds, which build up the continuity of the three-stranded β-sheets of each molecule, resulting in a six-stranded antiparallel pleated sheet extends over the dimer. We have also obtained a CTX A5 crystal that contains dimers under different crystallization conditions (data not shown). Therefore, all the reported CTX crystal structures appear to exhibit multimeric association, whereas structures obtained by NMR suggest the existance of CTX monomers below pH 6.0. It would be interesting to know if similar, even if only transient, molecular associations exist in solution or cell membranes. The H-bonds may not be strong enough to form a stable multimeric CTX molecule in solution, but the interactions might be sufficiently strong in the membrane environment.

Table 4: Intermolecular Hydrogen Bonds

molecule I···molecule II	bond distance (Å)
Cys44 O···Ser57 OG	2.84
Pro45 O···Ser57 OG	2.96
Lys46 NZ···Ser57 O	2.75
Asn47 N···Thr58 OG1	3.27
Cys55 N···Cys55 O	2.84
Cys55 O···Cys55 N	2.78
Ser57 O···Lys46 NZ	3.38
Ser57 OG···Pro45 O	3.47
Ser57 OG···Cys44 O	2.77

In order to see the folding topology of the subunits in the dimeric state, two different views of the dimer presented in the ribbon schematic diagram are shown in Figure 6, panels A,B. The view shown in panel B is obtained by rotating the figure in panel A by approximately 90° and emphasize the concavity of the CTX dimer. In Figure 6A, the tips of all three finger loops are facing outward and located along the two edges of the CTX dimer. It should be emphasized that the two subunits in the CTX dimer are not mirror images of each other (Figure 6B). They are aligned antisymmetrically with respect to the intermolecular H-bond interface (Figure 6A,C).

Most amino acid residues located on the concave side of the CTX dimer are positively charged (Figure 6). In contrast, all three acidic residues (Glu17, Asp42, and Asp59) are located on the convex side. Residues located near the tip of the loop are hydrophobic and form two parallel hydrophobic columns with length about 34 Å. Thus, the charged amino acids are polarized and distributed on two opposite sides of the hydrophobic column. The significance of these observations will be discussed later.

Crystal Packing. Monomers A and B are presented as two molecules in an asymmetric unit in Figure 7A. After these two molecules are rotated by 180° and translated a half unit cell along the *z* axis, monomers A and B become A′ and B′, respectively. This arrangement explains the presence of a peak at $U = 0.0$, $V = 0.0$, and $W = 0.5$ in the native Patterson map (data not shown). Although monomers A and B′ orient similarly, the two molecules are not identical.

The CTX dimer has 10 distinct contact regions between its subunits resulting in a total of 211 interactions ranging from 2.3 to 4.1 Å (Figure 7B). The contacts are dominated by the hydrophobic residues of three loops, excluding them from solvent interactions. Therefore, the dimer units assemble in the crystal mainly by loop-to-loop interactions. This observation reinforces the implication that the CTX A5 loops are reclined in a hydrophobic environment similar to that of the membrane core. Two other observations are in line with this suggestion.

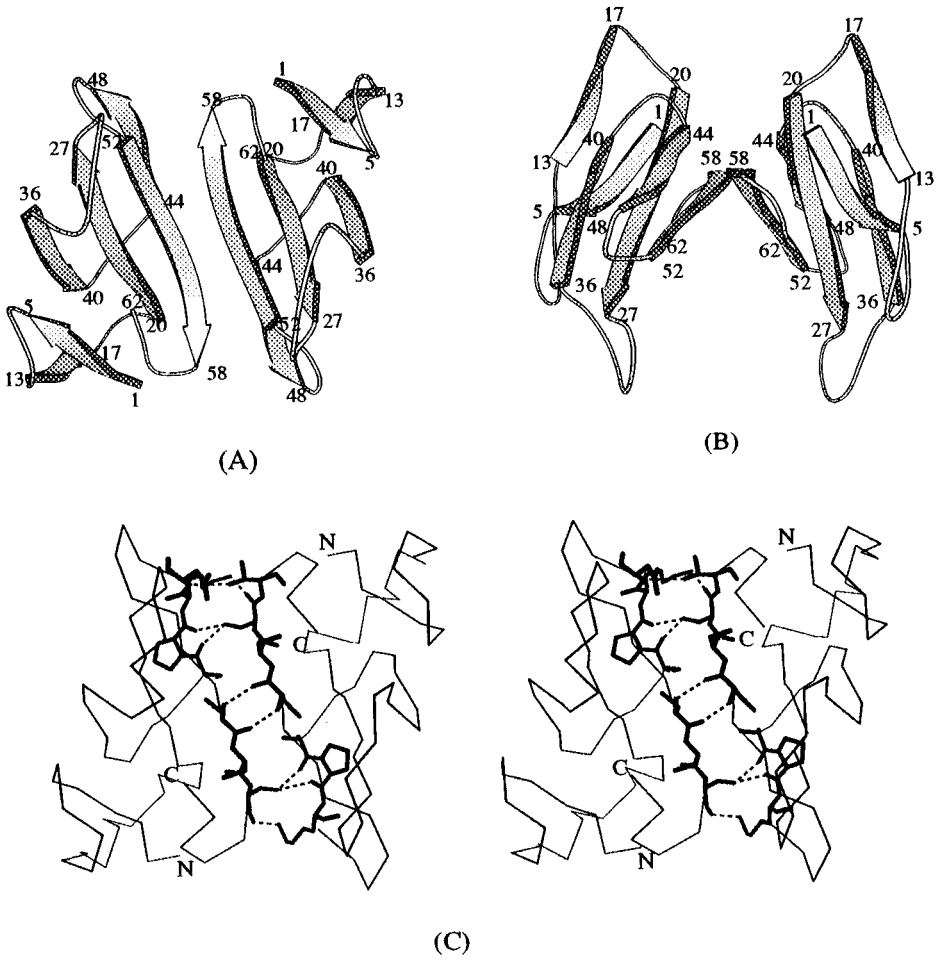

FIGURE 6: Dimeric structure of CTX A5. (A) Ribbon representation with the hydrophobic tips of the three finger loops facing out of the surface, (B) ribbon representation to emphasize the concavity of the dimer, and (C) stereo view of the dimer with nine hydrogen bonds.

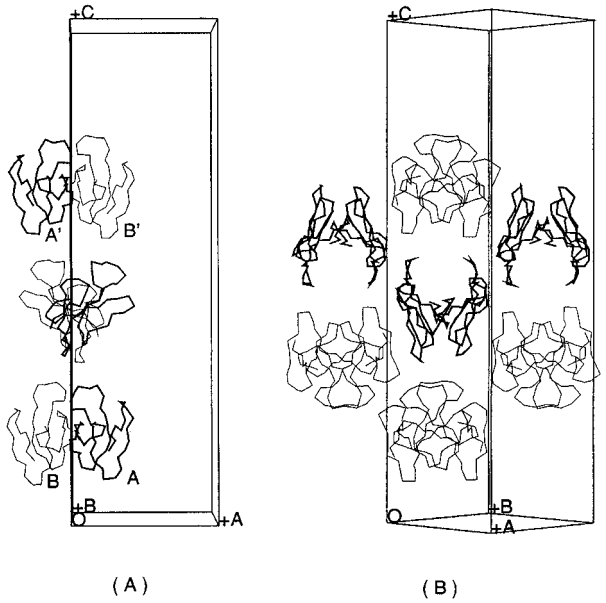

FIGURE 7: Crystal packing of CTX A5 dimer. Panel A shows the relative orientation of the two monomers in the crystals, and panel B emphasizes the hydrophobic contact between the hydrophobic amino acid residues near the tips of loop I and II.

First, a water molecule can be detected in tightening loop II by forming additional H-bonds between the NH of Leu27 and CO of Phe34 (Table 3). Consequently, the β-sheet content of CTX A5 in the crystalline state should be higher than that in solution. Available spectroscopic evidences have suggested that memebrane binding can cause an increase in β-sheet content of CTX A5. Therefore, the X-ray structure possibly resembles the membrane binding state of CTX A5.

Second, a continuous hydrophobic column is formed by residues Leu8, Pro9, Phe10, and Ile11 from loop I, Phe30, Pro31, Leu32, Lys33, Phe34, Pro35, and Val36 from loop II, and Ala49, Leu50, and Leu51 from loop III (Figure 8). This continuous hydrophobic region covers the longitudinal dimension of the CTX A5 molecule (34 Å). The hydrophobic region of a membrane bilayer has been shown to be 30∼35 Å in size (Whites & Wimley, 1994). We have probed the interactions of CTX A5 with perdeuterated PC bilayers by solid-state ^{2}H NMR. We observed enhanced order parameter profiles near the tail of fatty acyl chains under certain experimental conditions (Chiang et al., manuscript in preparation). Therefore, this hydrophobic column can serve as a membrane-spanning domain for the CTX−bilayer interactions.

Comparison with the NMR Structure of CTX A5. The NMR structure of CTX A5 has been determined at pH 3.7 (Singhal et al., 1993). A total of 445 experimentally derived NOE distance constraints and 27 ϕ angle constraints were used to calculate the solution structure of this molecule. As summarized in Figure 9, the overall three-dimensional structures of CTX A5 as determined by NMR spectroscopy and X-ray crystallography are similar. Even the hydrogen-bond patterns in the two β-sheets and the torsion angles in the β-turns 46−49 and 56−59 caused by the four disulfide bonds are found to be similar.

FIGURE 8: Comparison of the amino acid side-chain distribution in the NMR (light line) and X-ray (dark line) structures of CTX A5. A continuous hydrophobic column about 34 Å long can be observed in the X-ray but not in the NMR structure.

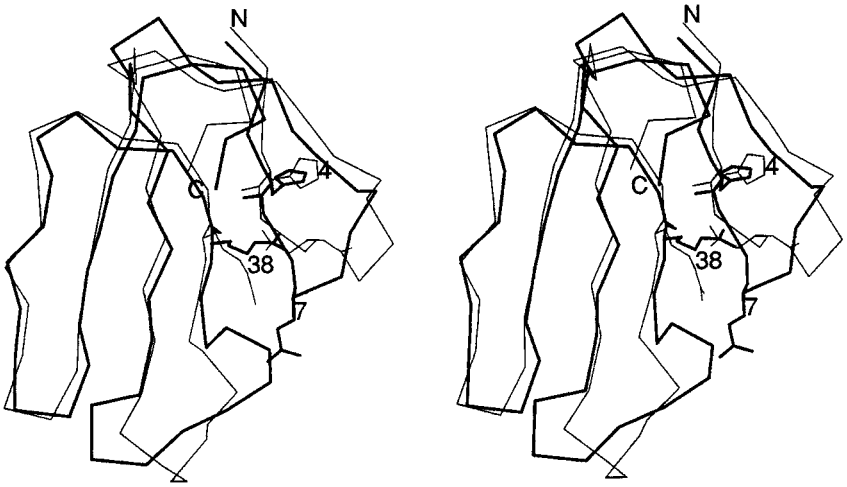

FIGURE 9: Comparison of the NMR (light line) and X-ray (dark line) structures of CTX A5 to emphasize the concerted side-chain reorientation during the protonation of the His4 imidazole ring.

We have, however, detected several interesting differences that might attribute to a conformational change in solution and/or different pH conditions. A least-squares fit of the NMR structure to that of the X-ray structure highlights the differences. The C_α rms distance of the NMR structure superimposed on the X-ray structure is 1.14 Å. The most significant difference was found at the tip of loop I (Gln7−Lys13) and in loop II (Lys28−Val36). This is due partially to the enhanced interaction between loops I and II in the crystalline state resulting from the extended Ω shape of the water-bound loop II.

The conformational inconsistency detected in the loop II region between the NMR and X-ray structure is interesting, since there is no titratable acidic amino acid residues in loop II. In fact, both NMR and X-ray structures are also available for toxin γ, a CTX homologue. The rms deviation of the main-chain atomic position of toxin γ among the three X-ray and nine best NMR structures is found to be higher than 5 Å for loop II. Therefore, the conformational flexibility of loop II may be mainly responsible for the structural differences among CTXs. It should be pointed out that the water molecule(s) detected in the X-ray structure of loop II is expected to undergo fast exchange in solution and may not be detectable by NMR. This might explain the taper-shaped loop II of the NMR structure, in contrast to the extended Ω loop of the X-ray crystal structure.

The difference detected near the tip of loop I can be explained by electrostatic interaction of the His4 imidazole ring under different protonation states with neighboring amino acid side chains. For the X-ray crystal structure, the deprotonated imidazole ring of His at pH 8.5 could be in proximal contact with the guanidino group of Arg38. They are separated by about 3.8 Å. In contrast, the NMR structure indicated that the protonated imidazole ring at pH 3.7 is ∼10 Å away from the guanidino group. The electrostatic repulsion between the side chain of His4 and Arg38 causes a conformational change and the side chain of Gln7 swung up to fill the space originally occupied by the guanidino group of Arg38 in the crystal structure. In addition, the side chains of residues 7−12 are reoriented. Such a concerted side-chain reorientation might disrupt the continuous hydrophobic column.

The orientation of the His4 imidazole ring as determined by NMR at pH 3.7 differs significantly from that detected by X-ray at pH 8.5 (Figure 9). This observation suggests the need for designing NMR experiment to check whether the disparities detected might be due to the different methodologies employed. The ring-current shift effect of imidazole is well-established and the observed reorientation of the imidazole side chain should shift the neighboring protons up/downfield. We therefore analyzed the ^{1}H NMR chemical shift differences of CTX A5 obtained at pH values

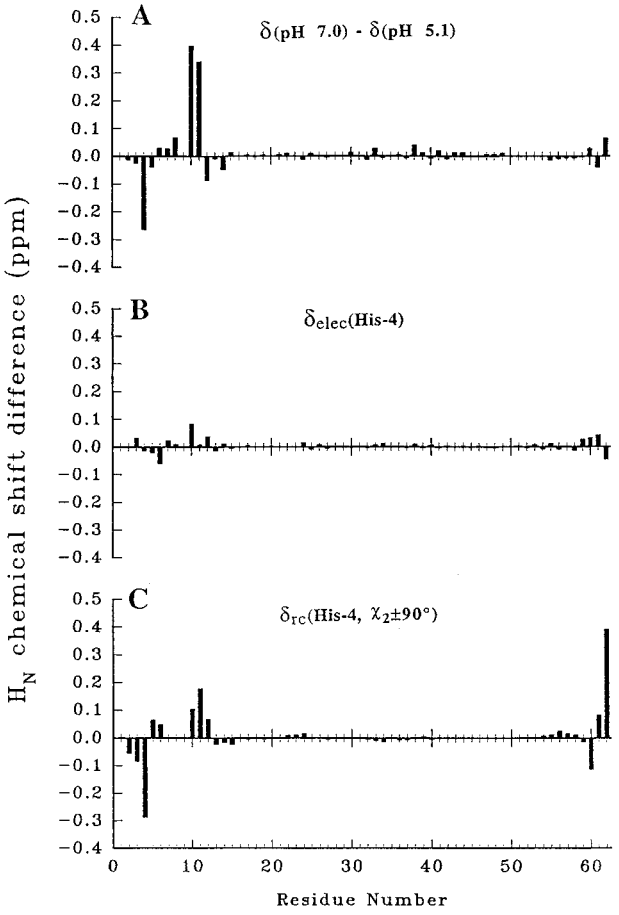

FIGURE 10: Analysis of ^{1}H NMR chemical shift differences of NH protons obtained at pH 7.0 and 5.1 as a function of amino acid positions of CTX A5: (A) experimental result as determined by ^{1}H NMR at 600 MHz (Chiang et al., 1996a), (B) estimation of electrostatic contribution to the chemical shift differences during the protonation of His4, and (C) estimation of the ring current effect on the chemical shift differences by assuming a reorientation of the imidazole ring at χ_2 angle (-C_β-Cγ-) by 90°.

below and above the pK_a of His4 (Figure 10). If reorientation of the imidazole ring indeed accompanies protonation, then the difference in ring-current effects should be detected by NMR at various amino acid positions. This was observed by Chiang et al. (1996a) and is reproduced here in Figure 10A.

To see whether the chemical shift differences are consistent with the side-chain reorientation depicted in Figure 9, we performed calculations to estimate both the electrostatic (δ_{elec}) and ring-current shift (δ_{rc}) effect on the amide protons of CTX A5 at various amino acid positions. As shown in panels A and C of Figure 10, a simple reorientation of the imidazole ring by 90° at χ_2 angle (-C_β-Cγ-) provides a reasonable simulation of the chemical shift differences measured between pH 7.0 and 5.1. In addition, the electrostatic contribution (Figure 10B) appears to be smaller than the ring-current effect. Therefore, consistency of the experimental and theoretical data in the loop I region indicates that the imidazole ring has indeed undergone reorientation at the studied pHs. Interestingly, chemical shift differences were also observed for residues near 32−37 and 54-62, although significant deviations between the theoretical and experimental results were obtained. The discrepancies might be due to the insufficiency of the theoretical model or the dynamics of the CTX A5 in solution. Nevertheless, the pH-induced conformational change of CTX A5 as suggested by the NMR and X-ray structures determined under different conditions is shown to be the result of intrinsic protonation of the His4 imidazole.

Comparison with X-ray Structure of Other CTXs. Comparing with other CTXs, the primary sequences of CTX A5 has two extra residues (refer to the alignment shown in Table 1). His4 and Leu32 are inserted in loops I and II, respectively. We have identified 32 conserved residues among CTX A5, CTX M3, and toxin γ. Sequence similarity among loop I and loop II is rather low (Table 1), suggesting that variations in the primary sequence of this region may also cause differences in the secondary structure. Sequence variation is in the order loop II > loop I > loop III.

The X-ray structure of CTX A5 shows similarities as well as differences with those of CTX M3 and toxin γ. The overall topology is the same among these three structures (Figure 11). The rms distances of the least-squares superposition of the C_α atoms of these three cardiotoxins are 0.51 Å (CTX A5−CTX M3), 0.92 Å (CTX A5−toxin γ), and 0.85 Å (CTX M3−toxin γ). Large differences in conformation among these three molecules occur at residues 5−12 and 26−36. Again, these residues are located in the loop I and II regions. The variation of the sequence with the rms deviation parallels that of the *B*-factor as indicated by the higher thermal parameters for these regions (Figure 5).

It has been shown that P-type CTX exhibits higher phospholipid binding activity than S-type CTX (Chien et al., 1994). CTX A5 and CTX M3 have overall structural similarity in their respective dimeric assembly. However, there are important structural differences between these two molecules (Figure 11A). First, as pointed out earlier, Pro31 of CTX A5 provides a water-binding site, which may stabilize the loop II conformation through H-bond formation. Second, the extended hydrophobic loop II of the CTX A5 molecule allows the formation of a continuous hydrophobic column involving all the hydrophobic residues of the three loops. This is not possible for the S-type CTX M3 because its loop is not only tapered but also hydrophilic.

Both CTX A5 and toxin γ are P-type CTX and contain a water-binding loop despite an amino acid insertion at position 32 for CTX A5. This insertion allows the clear detection of an Ω-shaped loop II and bridges the hydrophobic tip of loops I and III (Figure 11B). It also increases the flexibility of loop II as evidenced by the higher temperature factor of CTX A5 than toxin γ in the same region [compare Figure 5B of this work with Figure 6 in Bilwes et al. (1994)]. In Table 3, we compare the H-bond distance within the water-binding loop for toxin γ and CTX A5. The result indicates that the water-binding Ω shape in the loop II hydrophobic region may be a general feature of P-type CTXs in crystals.

DISCUSSION

The X-ray structure of CTX A5 at pH 8.5 described here provides a structural basis for the pH-dependent membrane-related activity of this molecule (Chien et al., 1991; 1993; Chiang et al., 1996a). The imidazole ring of His4 undergoes significant reorientation at different pH, as indicated by comparing the NMR and X-ray structures and confirmed by NMR chemical shift analysis. Concerted motion of other amino acid side chains near His4 has also been detected, suggesting that local conformational change(s) during His4

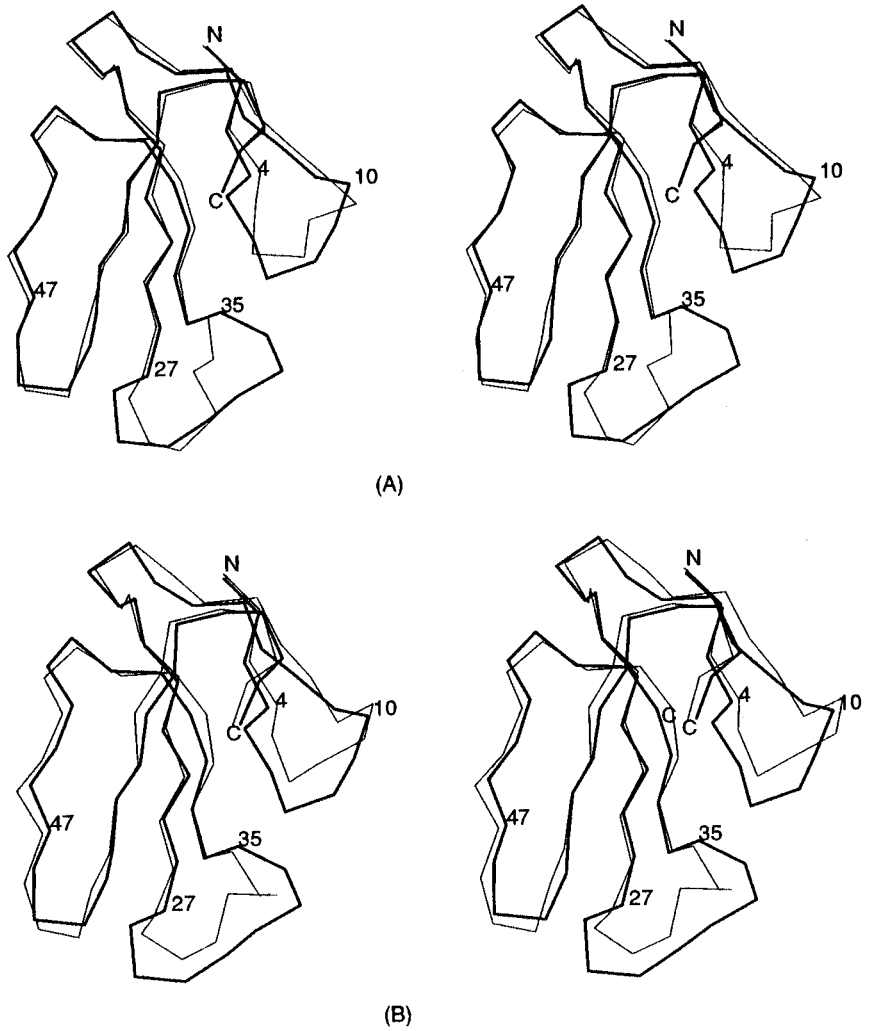

FIGURE 11: Comparison of the C_α backbone of CTX A5 (dark line) with CTX M3 (A) and toxin γ (B) (light lines) as determined by X-ray crystallography.

protonation might also be responsible for the pH-dependent binding ability of CTX A5 to membranes.

The X-ray structure appears to be a good model for the membrane-binding state of CTX A5. Examination of the crystal packing indicates that hydrophobic interactions similar to those in membrane bilayers may play a role in the formation of the water-binding loop. In particular, the extended Ω-shaped central loop of CTX A5, in conjunction with other hydrophobic residues near the tips of loop I and III, can form a hydrophobic column about 34 Å long. These observations are consistent with previous spectroscopic studies on the interactions of CTX with membranes. For instance, NMR studies indicated that the tips of the three-finger loops have been found to be most perturbed when toxin γ interacts with perdeuterated dodecylphosphocholine micelles (Dauplais et al., 1995).

It is interesting to point out that important structural modifications are usually found at the tip of loop II for toxins with three-finger loops. For instance, in sharp contrast to the extended Ω loop of CTX A5, the long-chain neurotoxins contain an additional disulfide bond to tighten the functionally important loop II region into a more tapered structure (Rees & Bilwes, 1993).

The newly identified continuous hydrophobic column formed by the three-finger loops not only may serve as a lipid binding site but also might penetrate membrane bilayers by forming multimers in cell membranes. A continuous hydrophobic stretch of residues like those in the helical and β-barrel structures of the photosynthetic reaction center and porin is usually identified as a membrane-spanning segment (Creighton, 1993). Herein, we suggest that a new transmembrane element other than helical or β-barrel structures is also possible. We propose that the transition between peripheral binding and penetration might be a general feature in the interaction of many amphiphilic polypeptides with membranes (He et al., 1995, 1996). The proposed structural transition may then explain the general cell-lytic effect of CTX molecules, which has led several previous investigators to name CTXs as direct lytic factors (Lee et al., 1979; Harvey, 1989, 1993).

We noted that there is some ambiguity in the proposed model. For instance, a wide distribution of positively charged residues can also be detected on the concave side of the dimer and separates the two continuous hydrophobic columns in the CTX dimer. Therefore, anionic lipids, carbohydrates, or other membrane polypeptides containing acidic amino acid residues are needed to stabilize the structure. Nevertheless, the proposed structural model probably explains why CTXs can show cell specificity, in addition to a general lytic effect, for several cell types such as cardiomyocytes. In fact, we have found recently that CTX can bind to sulfated oligosaccharides specifically and this

binding further enhances the lipid binding ability of snake CTXs as studied by Langmuir monolayer (Patel et al., 1997). We are currently investigating the detailed molecular interactions between sulfated oligosaccharide and CTX by using fluorescence, NMR, and X-ray techniques. The X-ray structure of CTX A5 should be a useful good starting point for research in this direction.

ACKNOWLEDGMENT

We thank Professor B. C. Wang for the initiation of the present work. Suggestions and editing from reviewers and Ms. Kavita Vyas are also deeply appreciated.

REFERENCES

Asakura, T., Taoka, K., Demura, M., & Williamson, M. P. (1995) *J. Biomol. NMR 6*, 227−236.

Bhaskaran, R., Huang, C.-C., Tsai, Y.-C., Jayaraman, G., Chang, D.-K., & Yu, C. (1994a) *J. Biol. Chem. 38*, 23500−23508.

Bhaskaran, R., Huang, C. C., Chang, D. K., & Yu, C. (1994b) *J. Mol. Biol. 235*, 1291−1301.

Bilwes, A., Rees, B., Moras, D., Ménez, R., & Ménez, A. (1994) *J. Mol. Biol. 239*, 122−136.

Brunger, A. T. (1990) *Acta Crystallogr., Sect. A 46*, 46−57.

Chiang, C.-M., Chien, K.-Y., Lin, H.-J., Lin, J.-F., Yeh, H.-C., Ho, P.-L., & Wu, W. (1996a) *Biochemistry 35*, 9167−9176.

Chiang, C.-M., Chang, S.-L., Lin, H.-j., & Wu, W (1996b) *Biochemistry 35*, 9177−9186.

Chien, K.-Y., Huang, W.-N., Jean, J.-H., & Wu, W. (1991) *J. Biol. Chem. 266*, 3252−3259.

Chien, K.-Y., Chiang, C.-M., Hseu, Y.-C., Vyas, A. A., Rule, G. S., & Wu, W. (1994) *J. Biol. Chem. 269*, 14473−14483.

Creighton, T. E. (1993) in *Proteins: structures and molecular properties*, W. H. Freeman and Co., New York.

Dauplais, M., Neumann, J. M., Pinkasfeld, S., Menez, A., & Roumestana, C. (1995) *Eur. J. Biochem. 230*, 213−220.

Dufton, M. J., & Hider, R. C. (1991) in *Snake venom* (Harvey, A. L., Ed.) pp 259−302, Pergamon Press, Inc., New York.

Fitzgerald, P. A. M. (1988) MERLOT, an integrated package of computer programs for the determination of crystal structures by molecular replacement, *J. Appl. Crystallogr. 21*, 273.

Gilquin, B., Roumestand, C., Zinn-Justin, S., Ménez, A., & Toma, F. (1993) *Biopolymers 33*, 1659−1675.

Harvey, A. L. (1985) *J. Toxicol. Toxin Rev. 4*, 41−69.

Harvey, A. L. (1991) in *Handbook of natural toxins* (Tu, A. T., Ed.) Vol. 5, pp 85−103, Marcel Dekker, Inc., New York.

He, K., Ludtke, S. J., Huang, H. W., & Worcester, D. L. (1995) *Biochemistry 34*, 15614−15618.

He, K., Ludtke, S. J., Heller, W. T., & Huang, H. W. (1996) *Biophys. J.* (in press).

Jahnke, W., Mierke, D. F., Beress, L., & Kessler, H. (1994) *J. Mol. Biol. 240*, 445−458.

Lee, C. Y., Ed. (1979) Snake Venom, *Handbook of Experimental Pharmacology*, Vol. 52, Springer-Verlag AG, Heidelberg, Germany.

Laskowski, R. A., MacArthur, M. W., Moss, D. S., & Thornton, J. M. (1993) *J. Appl. Crystallogr. 26*, 283−291.

Matthews, B. W. (1968) *J. Mol. Biol. 33*, 491−497.

Navaza, J. (1994) *Acta Crystallogr., Sect. A 50*, 157−163.

O'Connell, J. F., Bougis, P. E., & Wüthrich, K. (1993) *Eur. J. Biochem. 213*, 891−900.

Osapay, K., & Case, D. A. (1991) *J. Am. Chem. Soc. 113*, 9436−9444.

Otwinowski, Z. (1993) in Data Collection and Processing: Proceedings of the CCP4 Study Weekend (Sawyer, L., Isaacs, N., & Bailey, S., Eds.) pp 56−62, SERC, Daresbury Laboratory, Warrington, U.K.

Patel, H. V., Vyas, A. A., Vyas, K. A., Liu, Y.-S., Chiang, C.-M., Chi, L.-M., & Wu, W. (1997) *J. Biol. Chem.* (in press).

Rees, B., & Bilwes, A. (1993) *Chem. Res. Toxicol. 6*, 385−406.

Rees, B., Bilwes, A., Samama, J. P., & Moras, D. (1990) *J. Mol. Biol. 214*, 281−297.

Singhal, A. K., Chien, K.-Y., Wu, W., & Rule, G. S. (1993) *Biochemistry 32*, 8036−8044.

White, S. H., & Wimley, W. C. (1994) *Curr. Opin. Struct. Biol. 4*, 79−86.

Williamson, M. P., & Asakura, T. (1993) *J. Magn. Reson., Ser. B 101*, 63−71.

BI962594H